Int. J. Heat Mass Transfer. Vol. 24, No. 8, pp. 1381–1395, 1981.
Printed in Great Britain

0017-9310/81/081381-15 $02.00/0

COUNTERCURRENT FLOW OF AIR/WATER AND STEAM/WATER THROUGH A HORIZONTAL PERFORATED PLATE

S. G. BANKOFF,† R. S. TANKIN, M. C. YUEN and C. L. HSIEH†‡
Mechanical and Nuclear Engineering Department, Northwestern University, Evanston, IL 60201, U.S.A.

(*Received* 9 *July* 1980 *and in revised form* 9 *February* 1981)

Abstract—The onset of downwards penetration of a bubbly water pool above a perforated plate was studied with both air and steam upflows. An interpolative scaling length is developed empirically, which, when introduced into the Wallis countercurrent flow equation, fits the air–water data for a variety of perforated-plate geometries, as well as full-length tube bundle data with saturated water and steam. The same equation, when suitably corrected for steam condensation in the immediate neighborhood of the plate, fits the steam–water data also. Implications for the cooling of overheated nuclear reactor cores are discussed.

NOMENCLATURE

C_f, liquid specific heat;
C, dimensionless constant for perforated plate, equation (8);
C', dimensionless constant for vertical pipes or channels, equation (6);
D, diameter;
f, mixing efficiency of steam and cold water at plate, equation (10);
g, acceleration due to gravity;
k_c, $2\pi/t_p$, critical wave number based on plate thickness;
h_{fg}, latent heat of vaporization;
$\hbar$, input rate of enthalpy relative to saturated water;
H_{in}, height of inlet water tube;
H^*, dimensionless volumetric flux, equation (4);
J^*, dimensionless volumetric flux, equation (1);
j'_g, vapor velocity through holes;
j, volumetric flux;
K^*, dimensionless volumetric flux, equation (3);
L_1, Laplace capillary constant, equation (2);
L^*, bond number, equation (8);
n, number of holes;
T, temperature;
ΔT_{sub}, Liquid subcooling, $T_s - T_f$;
t_p, Plate thickness;
w, reference length, equation (5);
W, mass flow rate;
R_T, $C_f(T_s - T_f)W_f/h_{fg}W_g$, ratio of enthalpy flow rates of water and steam;
$R_{T,d}$, Ratio of enthalpy flow rates of water delivered through the plate (based on entrance conditions) and inlet steam, equation (12).

Greek symbols

β, exponent, equation (7);
γ, perforation ratio, area of holes/area of plate;
ρ, density;
σ, surface tension.

Subscripts

d, downwards delivery;
f, liquid;
g, steam or air;
e, effective;
in, inlet;
k, phase indicator, k = g or f;
s, saturated;
sub, subcooling;
u, upwards.

1. INTRODUCTION

WHEN GAS and liquid flow countercurrently under the influence of gravity in a vertical pipe, channel or through a perforated plate, a limiting condition known variously as flooding or CCFL (countercurrent flow limitation) is eventually reached as either the gas or liquid inlet flow is increased, keeping the other flow constant. This limitation determines the throughput capacity of various types of equipment, and hence has been extensively studied. Representatives of this work are the studies of sieve plate performance in mass transfer towers [1–4], and the more recent work simulating the injection of cold water into an overheated nuclear reactor core [5–8]. It is clear from just these two examples that a wide variety of phenomena are assumed under the topic of flooding, and a more detailed classification is required.

Three effects can be identified as being important in determining the stability of countercurrent flow. In

† Chemical Engineering Department.
‡ Present address: Walden Division, Abcor Inc., Wilmington MA 01887, U.S.A.

long vertical channels interfacial shear tends to dominate, and several studies [9–11] have examined the condition for instability of an interfacial travelling wave in an annular or flat-plate configuration. However, entrance and exit inertial effects can be very important, especially for short tubes. In perforated plates with zero or negligible condensation, these effects are probably dominant. Lastly, most studies have dealt with gas/liquid pairs, or vapor/liquid pairs which are nearly in thermodynamic equilibrium, so that interfacial mass transfer is either absent or else not important in determining the hydrodynamics. Recently, however, there has been considerable interest in steam/cold water, where rapid condensation can have a significant, and even dominant, effect in determining the stability of the flow.

An example where all three effects may be significant is the vertical countercurrent flow of steam and cold water through a horizontal perforated plate. This situation may be encountered at the upper tie plate of an overheated pressurized water reactor (PWR). The entrance of emergency core cooling system (ECCS) water into the core can then be impeded by the flow of rising steam from the hot fuel pin surfaces. Indeed, this is the motivation for this study. Another example is the injection of ECS water into the annular downcomer region of the same PWR, in an attempt to flood the overheated core from below. In a number of small-scale studies of this situation [12–15] the importance of condensation has been amply demonstrated. The point at which the entering water flow is just sufficient to condense all of the steam, assuming perfect mixing, represents an instability condition, in which water begins to be delivered downwards through the annulus, or end-of-complete bypass (EOCB) occurs. It turns out, however, that this criterion is not important in this study, for reasons to be explained below.

A major problem is the choice of appropriate length scales in order to allow prediction of inception of flooding (countercurrent flow instability), or inception of liquid downwards penetration (EOCB) in large-scale equipment from small-scale prototypical data. The importance of this is underscored by the highly informative LOFT (loss of fluid test) program [16]. One of the questions to be settled by this costly program, involving a one-eighth scale mock-up of a full scale PWR, was whether the annulus width or circumference is the appropriate length scale in determining the downcomer penetration. Two length scales have been generally available, corresponding to two dimensionless superficial velocities (or volumetric fluxes). One is the hydraulic diameter of the flow passage, leading to the widely-used J^* scaling introduced by Wallis [17]

$$J_k^* = j_k\left[\frac{\rho_k}{gD(\rho_f - \rho_g)}\right]^{1/2}; \quad k = f \text{ or } g \tag{1}$$

where j_k is the volumetric flux of the gas (g) or liquid (f), and D is the pipe or hole diameter, as the characteristic length of the flow cross-section. In large-scale equipment, however, the influence of the flow passage diameter becomes small, and another characteristic length has been constructed from the properties of the fluid–fluid interface. This length is the Laplace capillary constant

$$L_1 = \left[\frac{\sigma}{g(\rho_f - \rho_g)}\right]^{1/2} \tag{2}$$

incorporated by Kutateladze [18] in the dimensionless number

$$K_k^* = \left[\frac{\rho_k^2}{g\sigma(\rho_f - \rho_g)}\right]^{1/4}; \quad k = f \text{ or } g \tag{3}$$

which has been found to be useful in determining the stability of boiling and of CCFL [19]. In cases where both the interfacial properties and the characteristic diameter are important, no satisfactory means exists at present for interpolating between these two length scales. Following to some extent the work of Liu and Collier [20], a new dimensionless group

$$H_k^* = j_k\left[\frac{\rho_k}{gw(\rho_f - \rho_g)}\right]^{1/2} \tag{4}$$

is introduced here, where the interpolative length scale is

$$w = D^{1-\beta}L_1^{\beta} \quad 0 \le \beta \le 1 \tag{5}$$

and where the empirical exponent β is correlated for data on the particular geometry of interest. An empirical treatment of this sort is necessary because of the presence of at least two other geometrical ratios, one being the ratio of plate thickness to hole diameter and another the fraction of the plate area occupied by holes. A more detailed discussion is given in Section 3.

Wallis [17] derived a purely kinematic equation for countercurrent flow limitation, based on the assumption of a critical relative velocity between the phases which is independent of the void fraction α. This assumption is equivalent to a one-parameter (α) family of straight lines in the (j_g, j_f) plane, whose envelope, when made dimensionless, is

$$(J_g^*)^{1/2} + (J_f^*)^{1/2} = C'. \tag{6}$$

Here C' is a parameter of order unity, which depends on entrance and exit conditions and other geometric factors. Surprisingly, it turns out that this equation correlates the present data very well, with the substitution of H_k^* for J_k^*, and a geometrical parameter C, which is determined by the horizontal perforated plate configuration. Indeed, the same equation can be used to determine the onset of downward liquid penetration (EOCB) with saturated or superheated steam and with cold water at various temperatures, by subtracting the fraction of the steam which is condensed in the neighborhood of the perforated plate. Furthermore, the same correlation equation can be used to predict results for a range of perforation ratios and geometries. Thus, while the results are geometry-specific, it is hoped that this approach can be used fairly generally.

Finally some physical insight can be obtained into

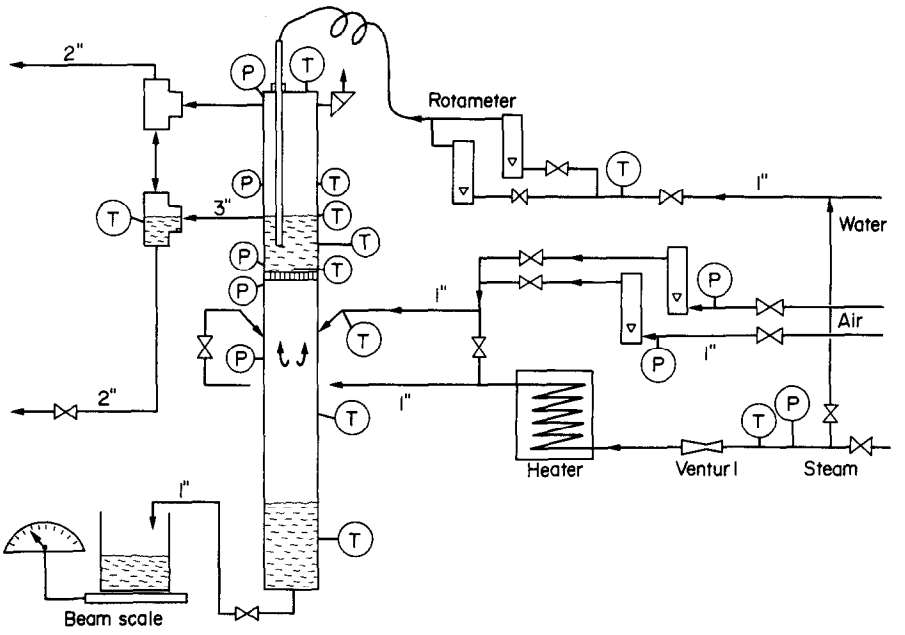

FIG. 1. Diagrammatic sketch of the perforated-plate air–water countercurrent flow systems.

the complex problem of penetration of cooling water downwards into a full-scale tube bundle from these results. Data obtained in countercurrent flow of saturated water and steam in a simulated full-length boiling-water reactor (BWR) tube bundle agree with the correlation developed herein, despite important differences in the physical mechanisms involved. From a consideration of these results one is led to some generalizations concerning countercurrent flow with interphase mass transfer in extended-surface systems.

2. EXPERIMENTAL APPARATUS AND PROCEDURE

The flow system (Fig. 1) allowed either saturated or superheated steam, or air, to be introduced below a horizontal perforated plate. Cold water entered the upper plenum chamber from a closed-end adjustable-height tube with horizontal spray holes and overflowed to drain. The height of the bubbly pool could be adjusted from 267 to 445 mm by moving the perforated plate. Various perforation geometries were tested (Fig. 2); the 15-hole geometry corresponds to a small

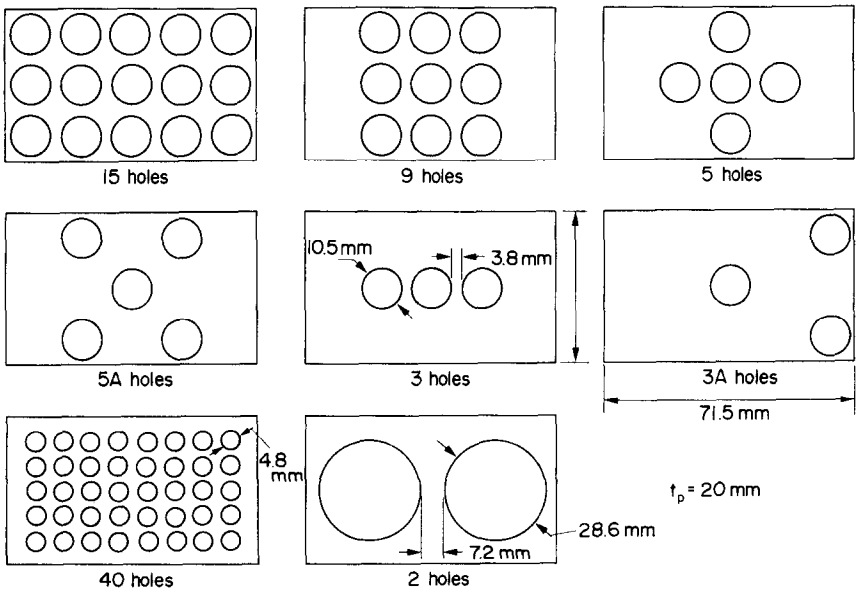

FIG. 2. Test plate perforation geometries.

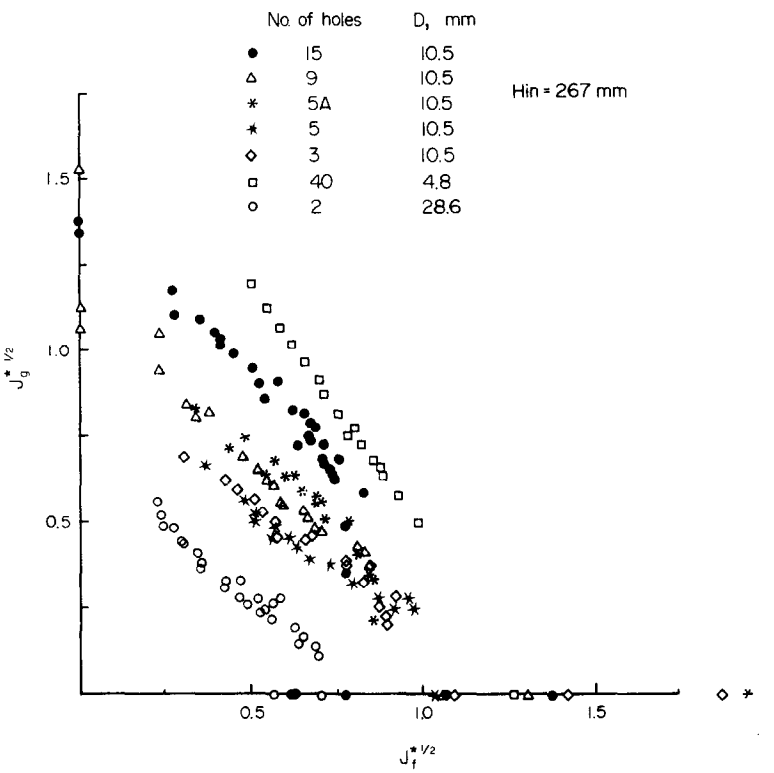

FIG. 3. J^* Scaling plot of air–water countercurrent flow data, equations (1) and (6).

segment of the upper tie plate of an actual pressurized-water reactor (PWR). The plate dimensions were 71.5 × 42.9 mm by 20 mm thick. Polycarbonate front and back plates were used in the test chamber to facilitate visual observation. The soft volume in the lower plenum could be varied by changing the height of the water drain tube. The inlet steam could be superheated by passing it through electrically heated stainless steel tubing. The water inlet flowrate was measured by two rotameters in parallel, and similarly the inlet air flow rate. To determine the void fraction in the bubbly pool two sensitive differential pressure transducers, with ranges of 0.15 to 3.6 kPa, were available for connection to a series of pressure taps along the side wall of the channel.

With air the procedure consisted of establishing the water inlet flow rate, and then increasing the air flow rate, determining the water delivery rate at each step, and finally the point of essentially zero downwards delivery (EOCB). With steam, the bubbly pool was first established at a steam flow rate greater than that required for complete bypass. The steam flow-rate was then gradually reduced at constant inlet water flow rate to determine EOCB.

3. AIR–WATER COUNTERCURRENT FLOW

One hundred and ninety-five data points were taken with air/water, using seven perforation geometries and two inlet water tube elevations. As shown in Fig. 3, plotting these data in the form of J_k^*, k = g or f [equation (1)] produces considerable scatter; although the expected slope of -1 [equation (6)] is obtained. Using the capillary constant L_1 as the characteristic length to plot the data in the form of K_k^* [equation (2)] reduces the scatter (Fig. 4) somewhat, but is still not satisfactory. An additional empirical parameter must be introduced, which is provided by the length scale given by equation (5). A trial function which is found to work very well is

$$\beta = \tanh(\gamma k_c D) \tag{7}$$

where the critical wave number $k_c \equiv 2\pi/t_p$, corresponds to the maximum wavelength which can be sustained on an interface of length t_p, the plate thickness; and γ, the perforation ratio, is the fraction of the plate area occupied by holes. Equation (7) has the desired property that $\beta \to 0$ as $D \to 0$, and $\beta \to 1$ as $D \to \infty$. From equations (1)–(5) this implies that H^* approaches J^* for small diameters and K^* for large diameters. However, the concept of an established, fully-developed annular flow with a critical relative velocity between the phases is clearly not applicable here (if ever), and these dimensionless functions should be regarded as following purely from dimensional analysis. Equation (7) also implies that H^* approaches J^* for small perforation ratios and large plate thicknesses, both of which approximate the long-tube geometry more closely. For large perforation ratios and thin plates, H^* approaches K^*; since an open-tank geometry is more closely approximated. However, the simple form of this trial function, with no adjustable exponents or coefficients, is noteworthy.

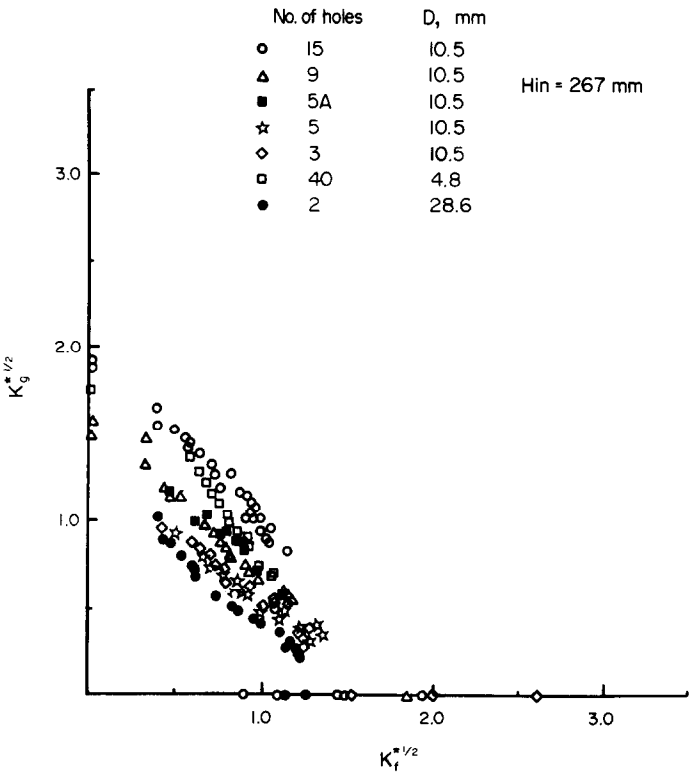

FIG. 4. K^* Scaling plot of air–water countercurrents flow data, equations (3) and (6).

The parameter C is a function only of geometry, and, as mentioned before, reflects entrance and exit effects. We have chosen to use the same function constructed by Sun [21] in correlating BWR (boiling water reactor) simulated bundle data obtained by Naitoh, Chino and Kawabe [22] and Jones [23] with saturated water and steam, in the hope of generalizing these results. This function, as shown in Fig. 5, is

$$C = 1.07 + 4.33 \times 10^{-3} L^* \quad L^* < 200$$
$$= 2 \quad L^* > 200 \tag{8}$$

where the Bond number L^* has been defined as $n\pi D[g(\rho_f - \rho_g)/\sigma]^{1/2}$ and n is the number of holes.

It is of considerable interest that the simple equation

$$H_g^{*1/2} + H_f^{*1/2} = C \tag{9}$$

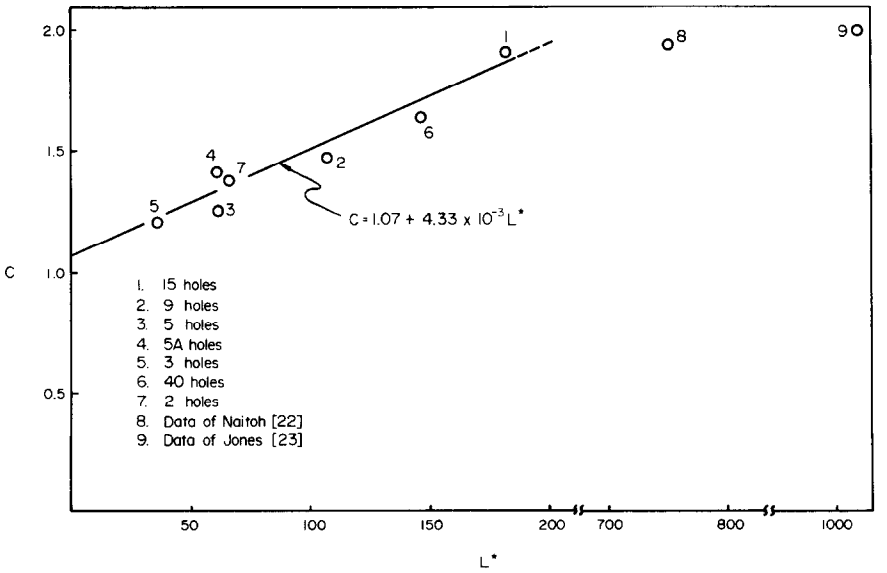

FIG. 5. Intercept C as a function of bond number for the present air–water data, and the steam-saturated water data of [22] and [23] in simulated boiling water reactor tube bundles, equation [8].

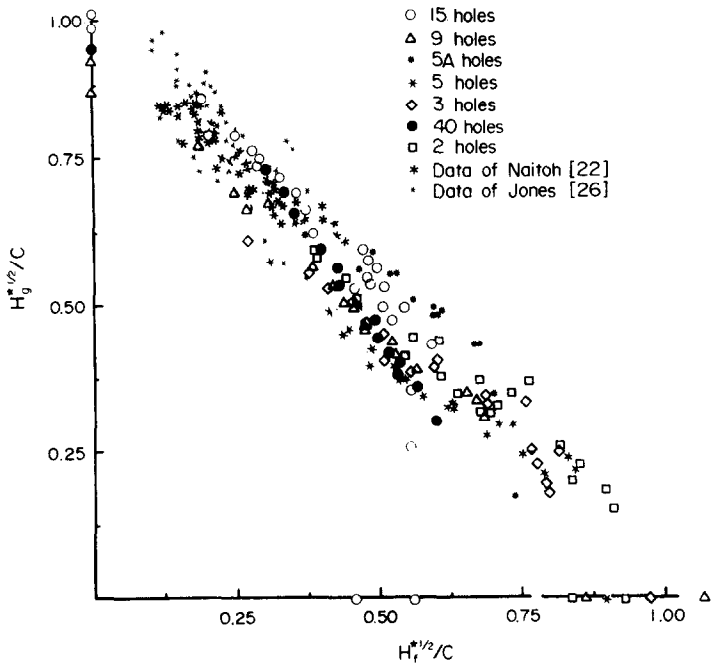

FIG. 6. H^* Scaling plot of air–water countercurrent flow data in seven perforated plate geometries, equations (6)–(9), and tube bundle steam-saturated water data compared to equation [9].

correlates all the present air–water data, as well as the previous steam–water data of Naitoh, Chino and Kawabe [22] and of Jones [23] in full-length tube bundles satisfactorily (Fig. 6). Furthermore, the effects of the inlet water elevation and of the lower plenum volume were both found to be negligible.

4. STEAM–WATER END-OF-COMPLETE-BYPASS (EOCB)

In these experiments a steam-supported water pool was established above the plate, and the steam flow rate was then slowly decreased until liquid penetration through the plate (end of complete bypass or, in chemical engineering terms, onset of weeping) was observed. Test ranges were T_g = 373–421 K; T_f = 285–359 K; number of holes (Fig. 2) 3–15; H_{in}, water inlet height above plate 5–710 mm.

Figure 7 shows the effect of ΔT_{sub} on EOCB for the 15-hole (PWR geometry) plate with inlet spray above

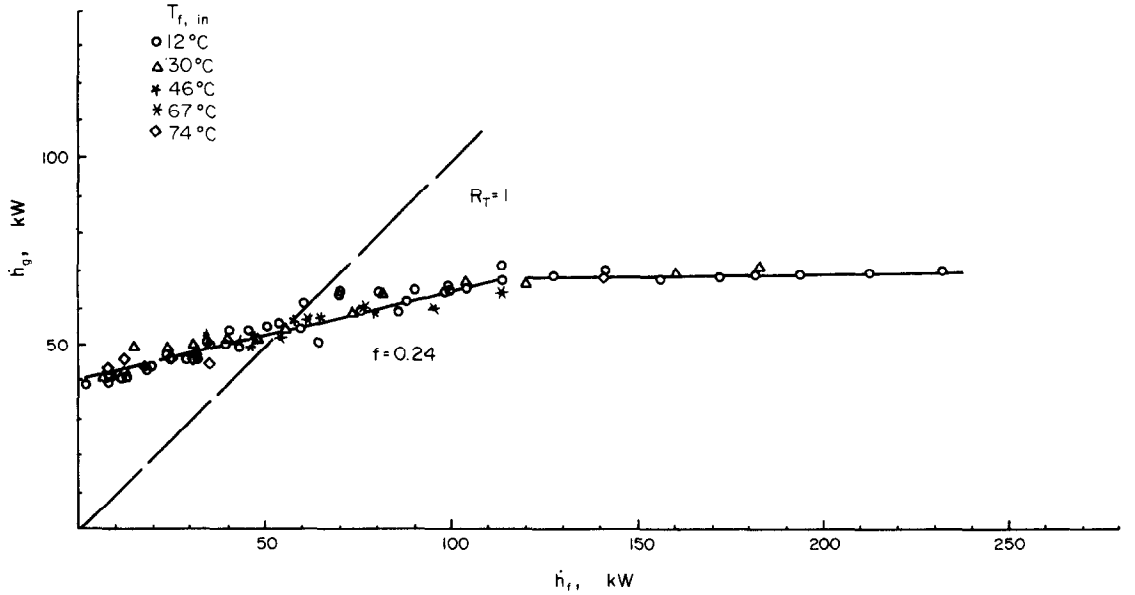

FIG. 7. Effect of liquid subcooling on EOCB (end of complete bypass) 15-hole data. Inlet water tube height above plate, H_{in} = 305 mm.

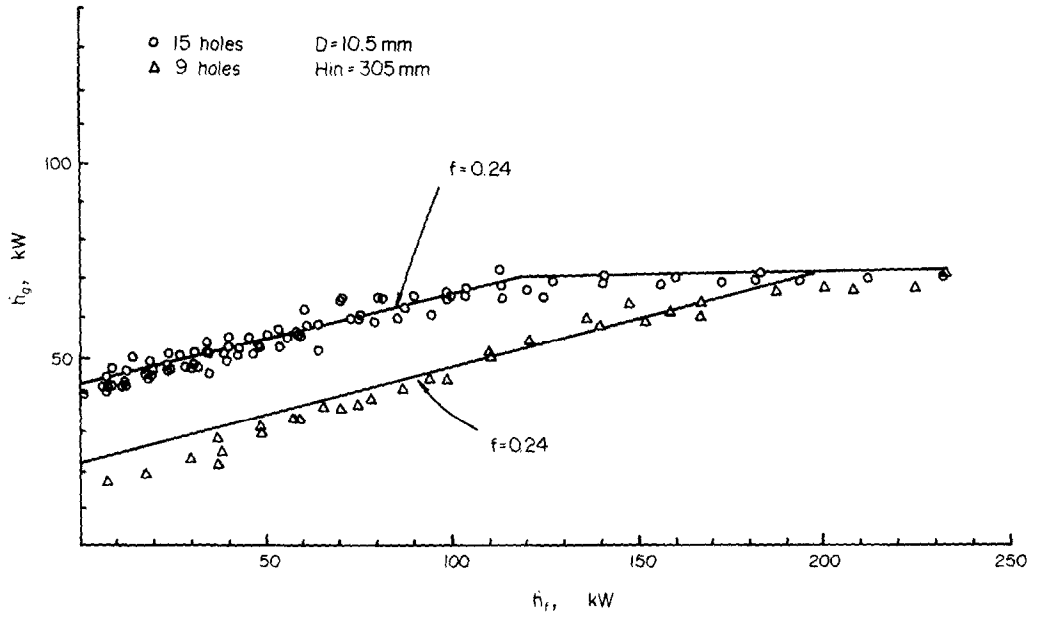

FIG. 8. Inlet enthalpy rates of steam and water at EOCB. 15-hole and 9-hole plate geometries, H_{in} = 305 mm.

the pool surface. The line $R_T \equiv C_f (T_s - T_f) W_f / h_{fg} W_g \equiv \dot{h}_f / \dot{h}_g = 1$, which represents thermodynamic equilibrium between the entering steam and water flows to produce only saturated water, is uncorrelated with these data. This differs from (water delivery, CCFL) data taken in tube bundles [22, 23] and scaled PWR downcomers [6], where this line represents an important stability threshold. The reasons for this difference will be discussed later. It is seen, first of all, that the EOCB correlation curve has a positive intercept, $\dot{h}_{g,\,min}$, as $\dot{h}_f$ approaches zero. This corresponds to a saturated-water pool above the plate, and hence approximates the air–water situation. With zero mass transfer the determining factor for downwards penetration of water is hydrodynamic, and not thermodynamic. As $\dot{h}_f$ increases from zero, a straight line is obtained, with positive slope. One can attribute the increased water flow as that necessary to condense the excess steam above $\dot{h}_{g,\,min}$. The slope, f, is thus a mixing efficiency for condensation of steam in the immediate neighborhood of the plate. There is a linear range for $\dot{h}_f < 120$ kW, which implies that the mixing efficiency is

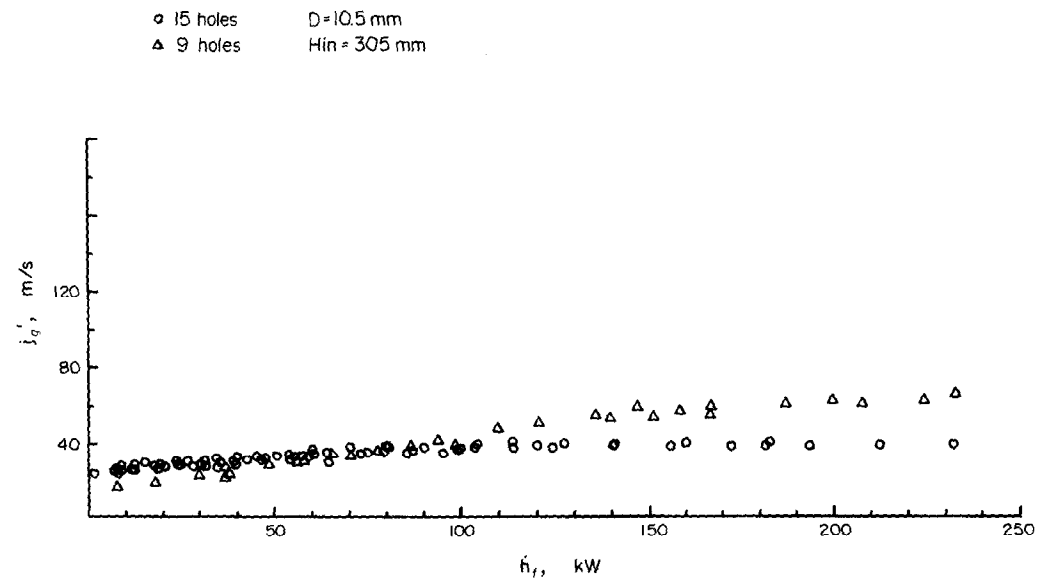

FIG. 9. Vapor velocity entering the holes, 15-hole and 9-hole data, H_{in} = 305 mm.

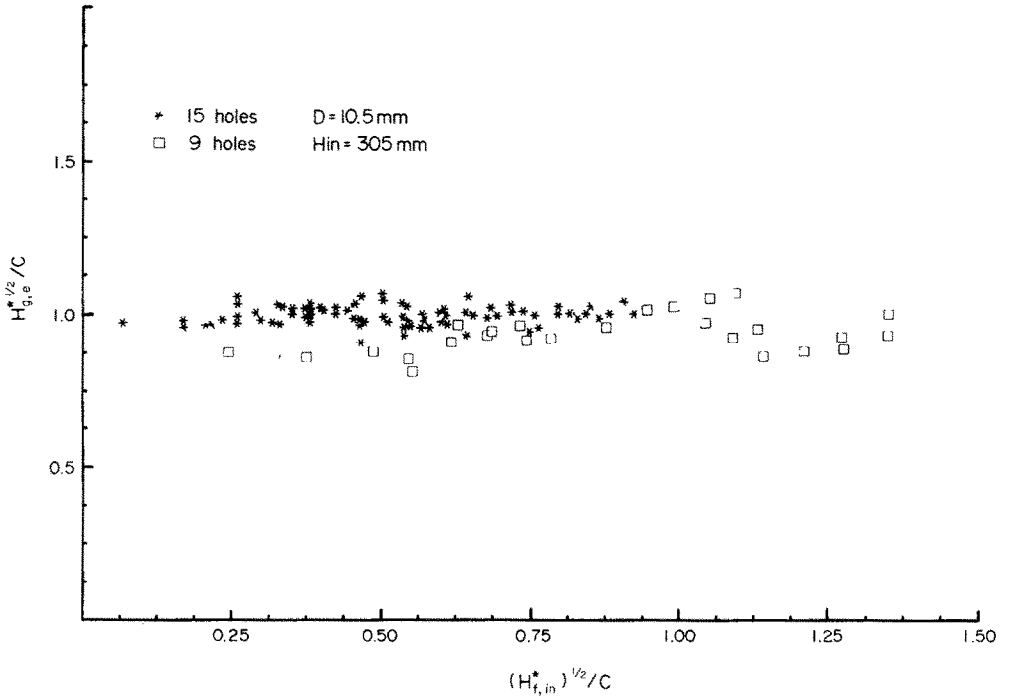

FIG. 10. Comparison of 15-hole and 9-hole data with EOCB correlation corrected for condensation, [equation (10)].

independent of the input flow rates in this range. For $\dot{h}_f > 120$ kW this linear mixing process becomes saturated, and excess water simply bypasses to drain. As $\dot{h}_f$ increases, the EOCB changes from a continuous leakage to oscillatory weeping, with a period ~1 s.

Similar data were taken with the 9-hole plate (Fig. 8), showing a similar slope ($f = 0.24$), but a lower intercept, in the linear range, but the same limiting value of $\dot{h}_g \sim 71$ kW for the saturation range. This suggests that the vapor velocity through the holes, j'_g, may be important in the linear range, which is verified by replotting the data in Fig. 9.

An effective dimensionless steam flowrate can now be defined as

$$H^*_{g,e} = H^*_g - \left(\frac{fC_f \Delta T_{sub}}{h_{fg}}\right)\left(\frac{\rho_f}{\rho_g}\right)^{1/2} H^*_{f,in} \quad (10)$$

which differs from the analogous quantity for PWR annulus flows [15] by the fact that f represents an efficiency for transport of cold water into the plate bubble boundary layer. However, f is not a free parameter chosen to fit the data, but is the (constant) slope of the $\dot{h}_f$ vs $\dot{h}_g$ curve in the linear range. From equations (9) and (10), the EOCB point, corresponding to the limiting case when countercurrent flow of steam and water through the plate just commences, is given by

$$H^{*1/2}_{g,e} = C. \quad (11)$$

Figure 10 shows that the steam-water EOCB data for two different perforation ratios, agree remarkably well with equation (11), which is deduced from air–water countercurrent flow data.

Similar runs were made with plates with smaller perforation ratios (Fig. 11) and $T_f = 285$ K, giving similar results; except that $f = 0.49$ and $\dot{h}_{g,max} = 62$ kW for 5 holes and 47 kW for 3 holes. The explanation for the improved mixing efficiency is believed to be the presence of large vertical standing eddies above the plugged-off regions, which help bring cold water down to the plate. This is shown by Fig. 12, where the EOCB point is no longer determined only by the steam velocity entering the holes, but now also depends on $\dot{h}_f$ and the perforation ratio. These data can also be correlated by equation (11), as shown in Fig. 13, although the spread is somewhat larger, in view of the great variation in plate geometry.

These data may be representative of EOCB behavior of the upper-head pool with elevated ECCS injection. To investigate the effect of bringing ECCS directly down to the tie plate, data were taken with horizontal injection of the water 5 mm above the plate. The effects of T_f are shown in Fig. 14. A marked improvement in liquid penetration ability is seen with $T_f = 285$ K. For $\dot{h}_f > 150$ kW two distinct modes of EOCB are observed. The higher mode, called oscillatory weeping, lies close to $R_T = 1$, which means that $f \sim 1$ for mixing of steam and cold water in the vicinity of the plate holes. Vapor-rich regions grow and collapse above the plate, resulting in inertial penetration of the holes. As the steam flow rate is reduced, the large scale growth and collapse ceases, and so does inertial penetration. Further reduction of steam flow leads to a nearly all-liquid pool, with high-speed

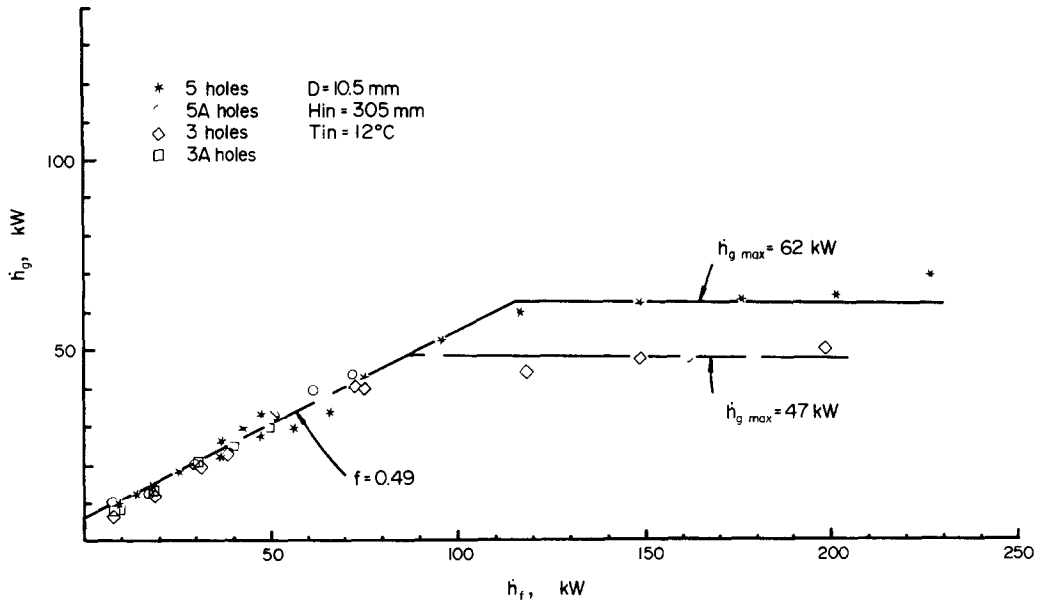

FIG. 11. EOCB data for 5-hole, 5A-hole, 3-hole and 3A-hole geometries. H_{in} = 305 mm; $T_{f,in}$ = 285 K.

bubble (or vapor jet) collapse in a thermal boundary layer near the plate (lower mode of EOCB). This is a stable region with no liquid penetration. Still further reduction of steam flow results in dumping of the entire pool into the lower plenum. The behavior at higher water temperatures was not investigated at these high values of $\dot{h}_f$ due to equipment limitations. The data at higher temperatures do not appear to follow the line $R_T = 1$ closely, indicating much less effective condensation at the holes.

This phenomenon with T_f = 285 K was explored more fully with different perforation ratios (Fig. 15). Here the R_T = 1 line (f = 1) is followed more closely with $f \sim 0.85$ for $\dot{h}_f < 9$kW, and $f \sim 0.63$ for $\dot{h}_f > 9$kW with $n < 15$. This shows again the powerful effect of the standing eddies above the blocked-off regions of the plate in bringing cold water back to the plate, and inducing excellent mixing in a thin layer above the holes. These eddies are very weak for the reference plate (n = 15), so that with low water flows ($\dot{h}_f <$ 4 kW) most of the steam–water mixing takes place away from the plate, even with H_{in} = 5–15 mm. Hence for this plate, the EOCB behavior in the $R_T < 1$ region is similar both for the high and low water inlet positions. In the $R_T > 1$ region, the two-mode behavior (for the same $\dot{h}_f$ one observes oscillatory

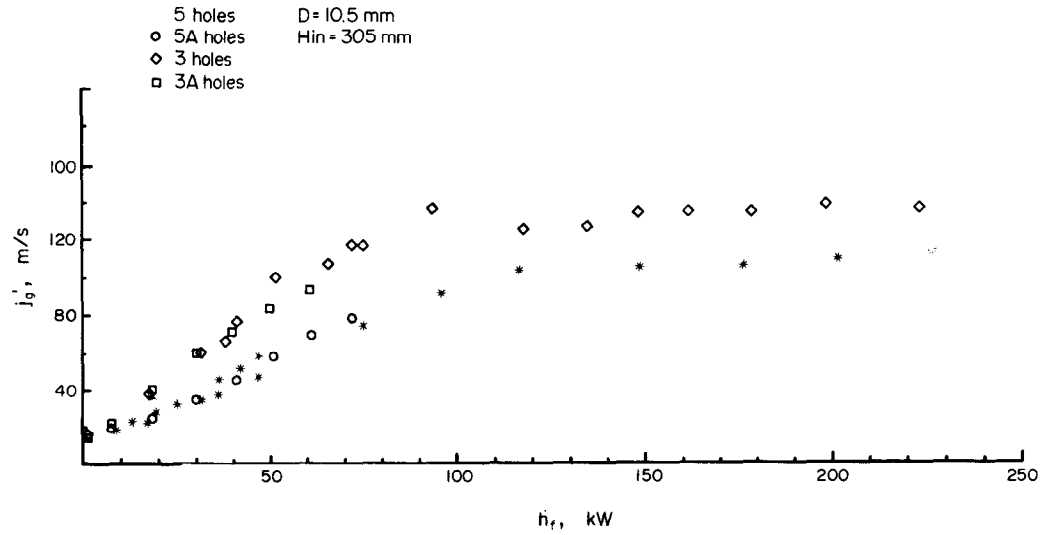

FIG. 12. Steam velocity entering holes for 5-hole, 5A-hole, 3-hole, and 3A-hole geometries [Refer to equation (2)]. H_{in} = 305 mm.

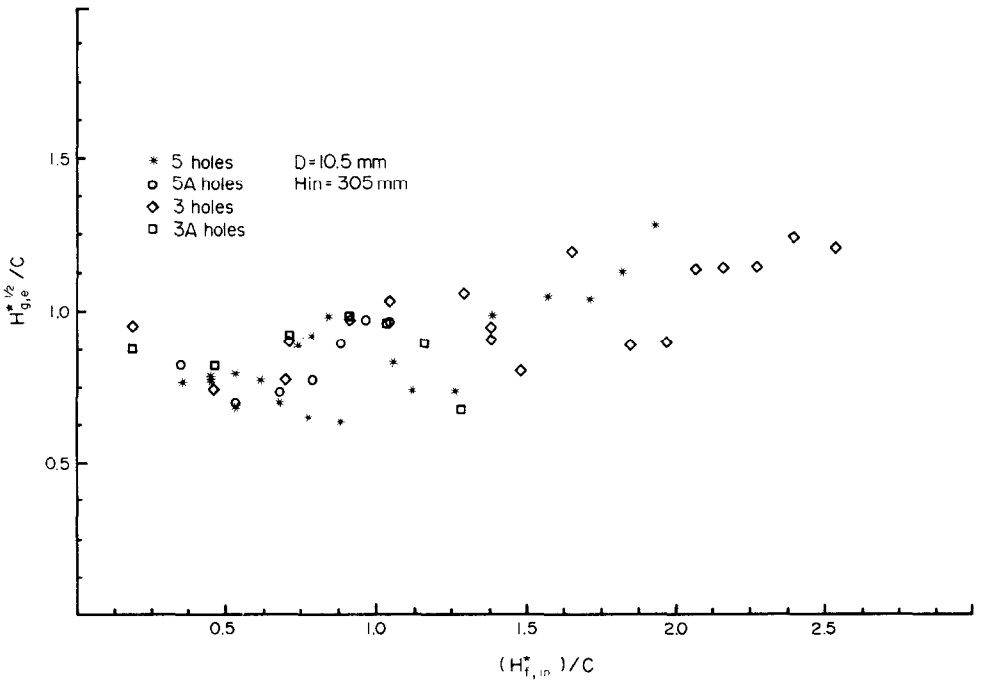

FIG. 13. Comparison of 5-hole, 5A-hole, 3-hole, and 3A-hole data with EOCB correlation, equation (10).

weeping at a high $\dot{h}_g$, dumping for a low $\dot{h}_g$; with a region of zero leakage in between) was exhibited (at all perforation ratios).

A rough estimate of the interfacial area in the bubble boundary layer above the plate can be made by assuming a hemispherical bubble to exist above every hole. The heat transfer coefficient for condensation can then be estimated from the steam flow rate and the water inlet temperature. This gives a range of condensation heat transfer coefficients of 1.1–1.8 $\times$ 10^6 W m^{-2} K^{-1} for these data for n = 3, 5, 9 and 15. This range agrees with condensation heat transfer coefficients measured by Bankoff and Mason [24] for single steam bubbles injected into a high-shear, cold

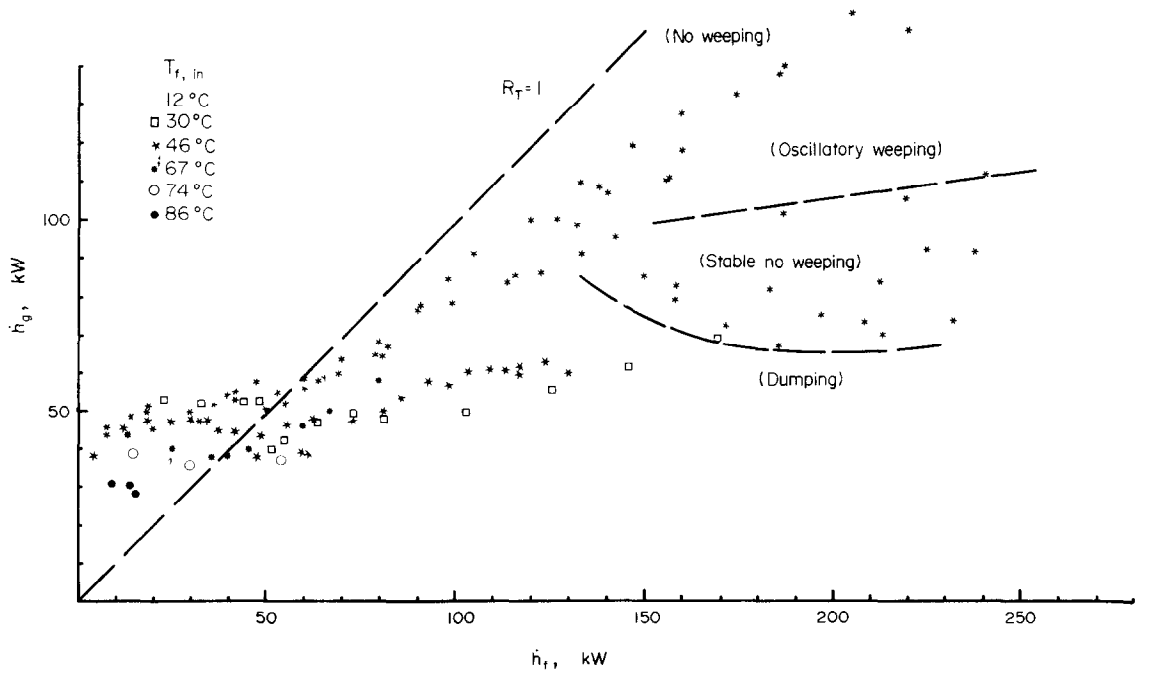

FIG. 14. 15-hole liquid penetration data obtained with water injected at plate. (EOCB) end of complete bypass ≡ dumping.

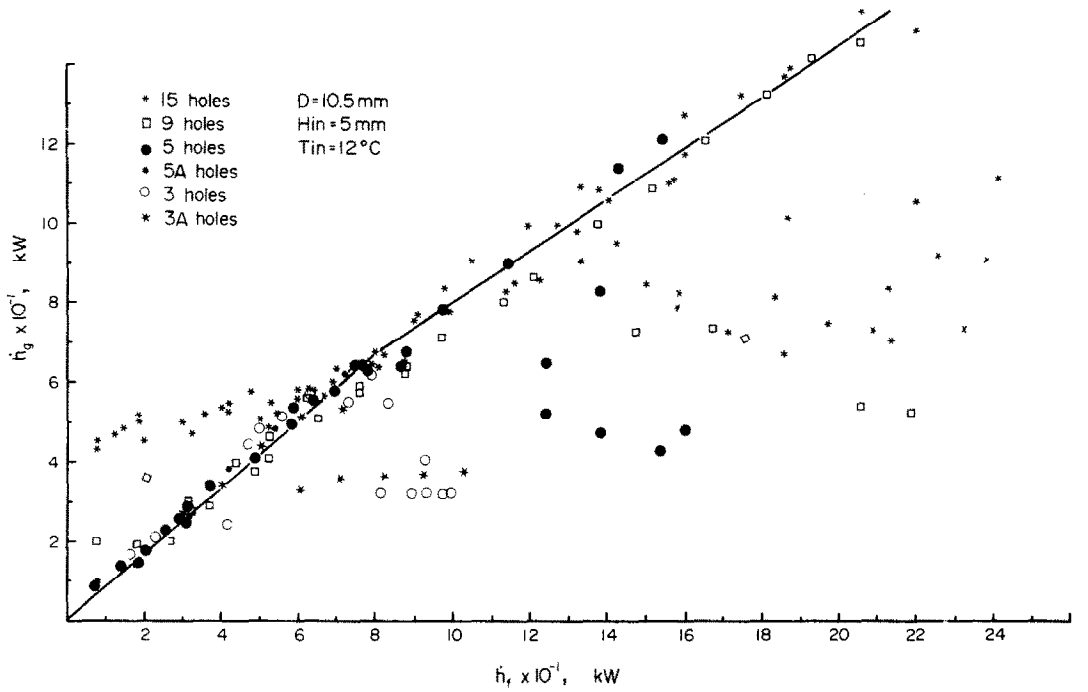

FIG. 15. Liquid penetration data with 285 K water injected at the plate (L_{in} = 5 mm) for various perforation ratios.

water region; and estimated by Merilo, Colah and Duffey [25] from data for transition to downflow for a steam–water bubbly pool.

It follows therefore that direct injection of cold water at the plate has a strong effect on EOCB, while water injected at higher elevations is much less effective. This is also shown by Fig. 16, where the 45° diagonal line (R_T = 1) is approximated only by cold water injected at the reference plate (n = 15). The situation is somewhat better for n = 9 (Fig. 17), since cold water can penetrate down along the walls more effectively.

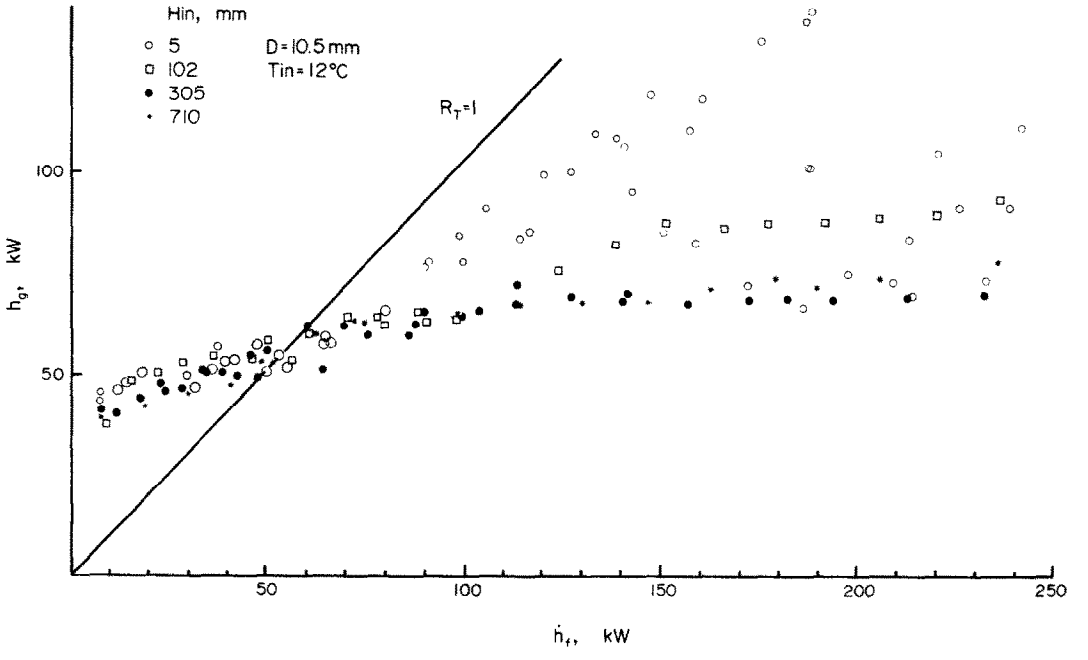

FIG. 16. Effect of liquid inlet spray nozzle position on EOCB, 15-hole data. $T_{f,in}$ = 285 K.

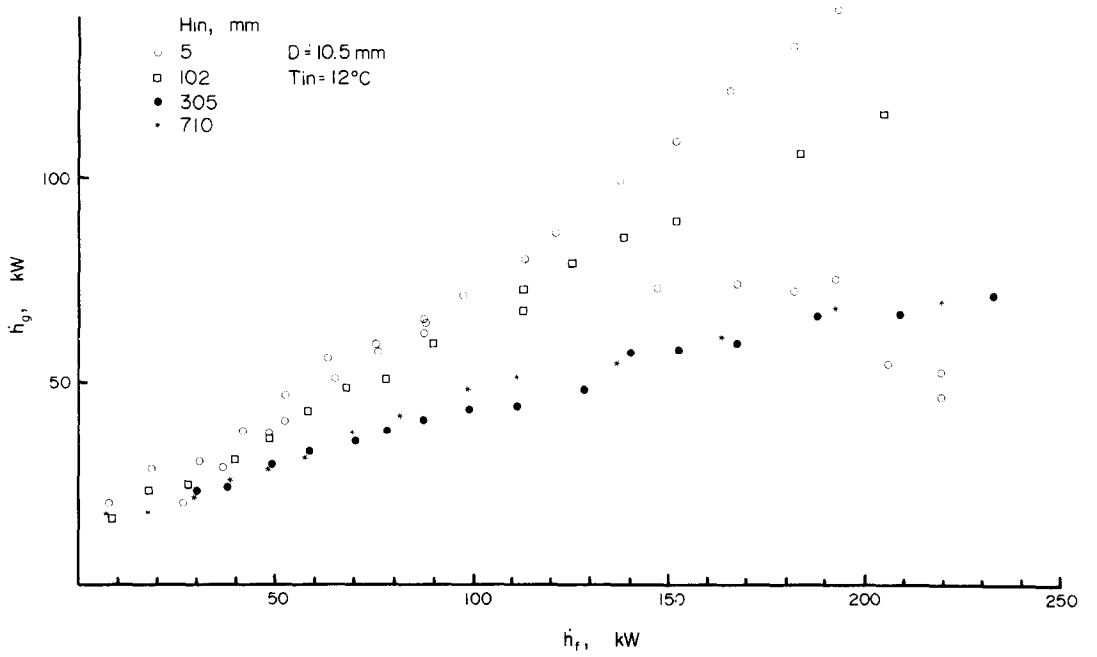

FIG. 17. Effect of liquid inlet spray nozzle position on EOCB, 9-hole data. $T_{f,in} = 285$ K.

5. APPLICATION TO REACTOR FLOODING

Although the present perforated plate steam water data deal only with EOCB (minimum $w_{g,in}$ such that $w_{f,d} = 0$, where $w_{g,in}$ and $w_{f,d}$ are the mass flow rates of steam in and liquid delivered), it is interesting to consider the reactor flooding problem by upper-head injection of ECCS water in conjunction with the data of Naitoh, Chino and Kawabe [22] and of Jones [23, 26]. These investigators measured $w_{f,d}$ vs $w_{g,in}$ with constant $w_{f,in}$ in unheated simulated BWR tube bundles, the steam being introduced at the bottom of the bundle. With saturated steam/water a delivery curve was obtained as a function of $w_{g,in}$, and was correlated by a Wallis-type equation [21], using K^* scaling and Bond number dependence of C. As shown above, we are able to correlate all their data, plus our own air/water data in a variety of perforated plate geometries, by a new scaling (H^*). In their cold water/steam experiments (CCFL) the line $R_T = 1$, corresponding to marginally complete condensation of all the steam in a perfectly mixed system, signals an important change in water delivery.

In the 'water-first' mode, delivery is complete as the steam flow is increased until the line $R_T = 1$ is reached. At this point some steam can reach the upper tie plate and reduces the downward water flow. However, any slight reduction in downward flow increases the steam flow reaching the plate, since the large tube bundle area guarantees excellent contact between the steam and water. This has a destabilizing effect, resulting in a jump to the CCFL line. Further increases in steam flow decrease $w_{f,d}$ until at the EOCB point, $w_{f,d} = 0$. On reversing the direction of traverse (steam-first mode) a hysteresis loop is obtained, since the jump point is now at $R_T > 1$. This is because the delivery through the holes in the neighborhood of $R_T = 1$ is saturated water, and it is not until the water delivery and the pool subcooling both increase, as $w_{g,in}$ decreases further, to some critical value, that subcooled water is drawn through the holes, producing a jump to full delivery.

It is thus clear that a two-dimensional flow map is inadequate, and a three-dimensional representation must be constructed for any particular flow system. One can define an additional thermodynamic quantity for each system

$$R_{T,d} = \dot{h}_{f,g}/\dot{h}_g = W_{f,d}\, C_f\, \Delta T_{sub}/h_{fg}\, W_g. \quad (12)$$

No steam reaches the holes in a simulated tube bundle experiment if $R_{T,d} > 1$, and hence there is complete delivery in this region. However, for a perforated-plate the delivered water may not be in thermodynamic equilibrium with the upflowing steam, so that steam can reach the holes for a limited range where $R_{T,d} = 1$. In this case the partial CCFL region extends past the line $R_{T,d} = 1$. The partial CCFL region has not been explored here experimentally, but it is suggested that an equation similar to equation (9) may hold

$$H_{g,e}^{*1/2} + H_{f,d}^{*1/2} = C \quad (13)$$

where $H_{g,e}^*$ is defined by equation (10) and C is given by equation (8). For the purposes of this discussion the exact form of the partial CCFL equation is not needed.

The complete bypass region is

$$H_{g,e}^{*1/2} \geq C. \quad (14)$$

For $H_{g,e}^{*1/2} < C$ and $R_{T,d} < 1$ equation (13) holds. The

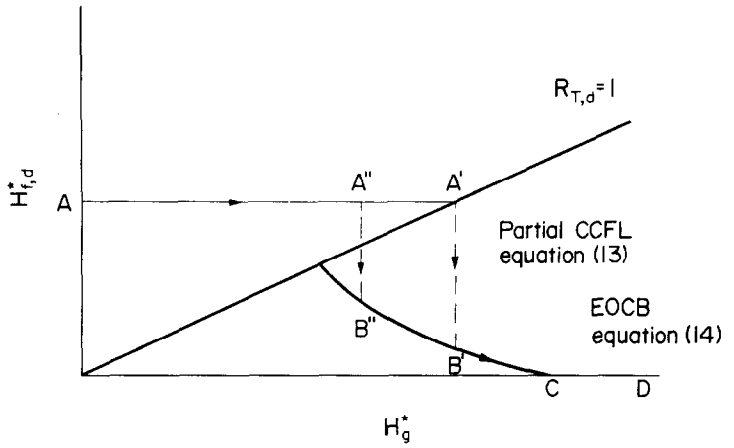

FIG. 18. System behavior, water-first mode of operation (Fixed $H^*_{f,in}$), unheated tube bundle or perforated plate.

details, however, are different for a perforated plate with or without an unheated (or heated) tube bundle, as well as for the steam-first or water-first modes of operation. It is therefore difficult to represent the three-dimensional flow map in the $H^*_g - H^*_{f,in} - H^*_{f,d}$ space. It is easier to visualize the locus of the system at constant H^*_g or constant $H^*_{f,in}$, corresponding to either the steam or water inputs being held constant, while the other independent variable is manipulated.

Figure 18 shows a cross-section of the three-dimensional flow map at constant $H^*_{f,in}$. In this case the water flow is first established, and steam flow is then begun. Initially, therefore, the system is at point A, corresponding to full delivery, and then moves along the line AA'. However, the behavior is now different for an unheated tube bundle and a perforated plate. We postpone the discussion of the heated tube bundle until later. For the unheated tube bundle no steam can reach the upper tie plate until $R_{T,d} = 1$ (point A'). At this point a jump occurs to B' on the partial CCFL line, since the 'choke point' (defined as the location where CCFL is most likely to occur) shifts from the bottom of the tube bundle to the upper tie plate. Further increases in steam flow cause further decreases in water delivery until the point C is reached, corresponding to zero delivery of water. The point C is the EOCB point, since increases in steam flow result in complete bypass of entering water (line CD). For a perforated plate, however, the system locus is slightly different. The jump to the partial CCFL line occurs at A'' to B'', since subcooled water can be delivered through the plate, even for $R_{T,d} > 1$. For a tube bundle the large surface area implies equilibration between the incoming steam and the downflowing water. For a perforated plate the choke point is, of course, always at the plate, but for a tube bundle, the choke point is initially at the bottom,

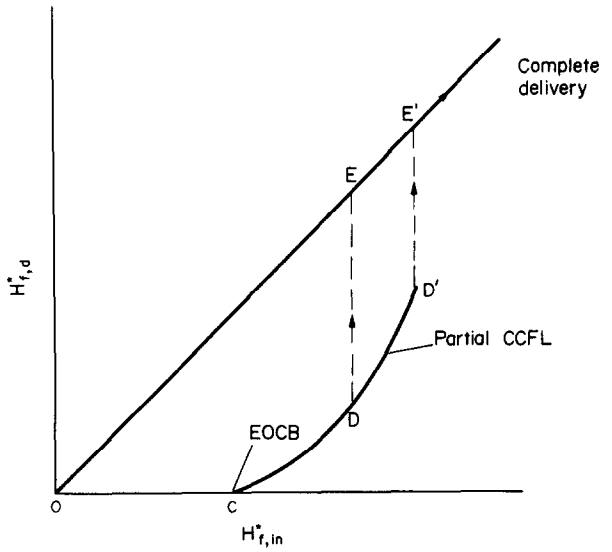

FIG. 19. System behavior, steam-first mode of operation (fixed H^*_g), unheated tube bundle or perforated plate.

where the steam velocity is maximum, but moves to the top once steam reaches the upper tie plate. This jump behavior has been observed by Jones [26] and Naitoh, Chino and Kawabe [22]. If the water inlet flow is changed, points A and C will both be different, although the line $R_{T,d}$ remains unchanged. There is thus a family of flow paths, which together make up the three-dimensional flow surface for the water-first mode.

In the steam-first mode (Fig. 19) the inlet steam variable H_g^* is fixed, so that the slice is taken in the $H_{f,d}^*$ plane. The line OEE′ represents complete delivery, while the positions of the constant lines $R_{T,d} = 1$ and $R_T = 1$ depends upon the inlet steam flowrate. As the water flow is increased, the path moves along the line OC until EOCB (point C) is reached. The unheated tube bundle follows the partial CCFL curve until $R_T = 1$, or slightly past this line (point D). This is a hysteresis effect due to the fact that cold water must penetrate down to the tie plate before full delivery can occur. At this point the flow is unstable. A small increase in cold water passing through the upper tie plate decreases the steam flow to the tie plate, since excellent contact is maintained in the tube bundle. A jump therefore occurs to the full delivery line (point E). For the perforated-plate, however, the hysteresis may be larger, since subcooled water can leave the system (D′ to E′). If $R_T > 1$ at C, then EOCB may nearly coincide with full delivery.

Some words of caution should be expressed at this point. In the unheated tube bundle studies, as well as our own studies, W_g, and hence H_g^*, is a fixed input variable. With hot dry surfaces below the tie plate, however, water penetrating down no longer has the destabilizing effect of reducing the steam flow to the plate. Instead, there is a feedback between $W_{f,d}$ and $W_{g,u}$, where $W_{f,d}$ is the water flowing downwards from the plate, and $W_{g,u}$ is the steam flowing upwards to the plate. When the EOCB is reached, ($W_{f,d} > 0$) water penetrating downwards results in an increased steam flow upwards, so that complete bypass is re-established. One can therefore expect the system to oscillate around the EOCB point for some time, unless delivery incoherencies are established due to scale effects, radial non-uniformities of rod temperatures, and/or ECCS inlet design.

6. CONCLUSIONS

A new scaling parameter, H^*, has been proposed which interpolates between the J^* and K^* parameters, and which may therefore be generally useful for CCFL studies. Applied to horizontal perforated plates and to unheated full-length tube bundles with no interfacial mass transfer, the simple equation (9) correlates a wide variety of data satisfactorily. With condensing mass transfer, the same equation can be used to predict the onset of downwards penetration, or end-of-complete bypass (EOCB), using an effective $H_{g,e}^*$ [equation (10)]. The application for the full CCFL region with condensation has not been studied. The mixing efficiency, f, is a constant, which is obtained experimentally. Applications to reactor flooding are discussed. The EOCB point is particularly significant in this case, since it will be stabilized by evaporation of water which has penetrated the upper tie plate and impinged on the hot surfaces. Further studies on this effect are indicated.

Acknowledgement—This work was supported by the U.S. Nuclear Regulatory Commission, and was presented at the Seventh International Light-Water Reactor Safety Information Meeting, Gaithersburg, MD (1979).

1. P. D. Jones and M. Van Winkle, Variables in perforated-plate column efficiency and pressure drop, *Ind. Engng Chem.* **49**, 232–238 (1957).
2. H. E. Eduljee, Design of sieve-type distillation plates, *Brit. chem. Engng* **4**, 320–326 (1959).
3. J. A. Davies, What to consider in your fractionator tray design, Part 2. Perforated trays, *Petrol/Chem. Engr* **2**, 250–253 (1961).
4. E. Showkry and V. Kolar, On the hydrodynamics of sieve plates without downcomers, *Chem. Engng J.* **8**, 41–51 (1974).
5. J. A. Block and C. J. Crowley, Effects of steam up-flow and superheated walls on ECC delivery in a simulated multiloop PWR geometry, Creare TN-210 (1975).
6. J. A. Block and P. H. Rothe, Progress on ECC bypass scaling, Creare TN-272, NUREG/CR-0048, R-2 (1977).
7. R. A. Cudnik, R. P. Collier, R. C. Dykhaizen, L. F. Flanigan and J. S. Liu. Steam-water mixing and system hydrodynamics program, Task 4, Battelle-Columbus Laboratories, NUREG/CR-0147, BMI-2003 (1978).
8. H. J. Richter and S. L. Murphy, Effect of scale on two-phase countercurrent flow flooding in annuli, Final Report, Dartmouth College, Hanover, N. H., NUREG/CR-0822 (1978).
9. Y. Zvirin, R. B. Duffey and K. H. Sun, On the derivation of a countercurrent flooding theory, presented at A.S.M.E. Mtg., N.Y. (1979).
10. A. G. Cetinbudaklar and G. I. Jameson. The mechanism of flooding in vertical countercurrent two-phase flow, *Chem. Engng Sci.* **24**, 1669–1680 (1969).
11. G. J. Jameson and A. G. Cetinbudaklar, wave inception by air flow over a liquid film, pp. 271–282, in *Cocurrent Gas–Liquid Flow*, edited by E. Rhodes and D. S. Scott), Plenum Press, New York (1969).
12. R. A. Cudnik and R. O. Wooton, Penetration of injected ECC water through the downcomer annulus in the presence of reverse core steam flow, Battelle-Columbus Laboratories Report (1974).
13. E. A. Harvego and P. North, Investigation of condensation phenomena in the semiscale mod-1 system, pp. 99–106, in *Topics in Two-Phase Heat Transfer and Flow* (edited by S. G. Bankoff). A.S.M.E., New York (1978).
14. J. S. K. Liu, R. P. Collier and R. A. Cudnik, Flooding of counter-current steam-water flow in an annulus, pp. 107–113, in *Topics in Two-Phase Heat Transfer and Flow* (edited by S. G. Bankoff). A.S.M.E., New York (1978).
15. J. A. Block, Condensation-driven fluid motions, *Int. J. Multi-phase Flow* **6**, 113–129 (1979).
16. G. D. McPherson, Heat and mass transfer lessons learned from the LOFT program, Invited lecture, *International Center for Heat and Mass Transfer, Seminar on Reactor Safety Heat Transfer*, Dubrovnik, Yugoslavia (1980).
17. G. B. Wallis, *One-Dimensional Two-Phase Flow*. McGraw-Hill, New York (1969).
18. S. S. Kutateladze, Heat transfer in condensation and boiling, USAEC Rpt. AEC-tr-3770 (1952).
19. O. L. Pushkina and Y. L. Sorokin, Breakdown of liquid

film motion in vertical tubes, *Heat Transfer—Soviet Research* **1**, 56 (1969).
20. J. S. K. Liu, R. P. Collier, Steam-water mixing and system hydrodynamics program, Quarterly Progress Report, Jan–Mar. 1979, NUREG/CR-0897, BMI-2029, Battelle Columbus Laboratories (1979).
21. K. H. Sun, Flooding correlations for BWR bundle upper tieplates and bottom side-entry orifices, *Second Multi-Phase Flow and Heat Transfer Symposium—Workshop*, Miami Beach, Florida (1979).
22. M. Naitoh, K. Chino and R. Kawabe, Restrictive effect of ascending steam on falling water during top spray *emergency core cooling, J. nucl. Sci. Tech.* **15**, 806 (1978).
23. D. D. Jones, Test report TLTA components CCFL tests, General Electric Company, NEDG-NUREG-23732 (1977).
24. S. G. Bankoff, and J. P. Mason, Heat transfer from the surface of a steam bubble in turbulent subcooled liquid stream, *A.I.Ch.E. Jl* **8**, 30–33 (1962).
25. M. Merilo, M. Colah and R. B. Duffey, Condensation induced transition from bubbling to liquid downflow in a turbulent two-phase pool, 18th Nat. Heat Transfer Conf., San Diego (1979).
26. D. D. Jones, Subcooled counter-current flow limiting characteristics of the upper region of a BWR fuel bundle, General Electric Co., Nuclear Systems Products Division, BD/ECC Program, NEDG-NUREG-23549 (1977).

ECOULEMENTS A CONTRECOURANT AIR/EAU ET VAPEUR D'EAU/EAU A TRAVERS UNE PLAQUE PERFOREE HORIZONTALE

Résumé—La pénétration d'une piscine d'eau au-dessus d'une plaque perforée est étudiée avec l'air et la vapeur d'eau en écoulement ascendant. On développe empiriquement une échelle de longueur qui lorsqu'elle est introduite dans l'équation de Wallis, décrit les données air–eau pour une variété de géométries de plaques perforées, aussi bien que des données pour la grappe de tubes avec de la vapeur d'eau et de l'eau saturée.

La même équation, corrigée convenablement pour la condensation de vapeur dans le voisinage immédiat de la plaque, représente aussi les données vapeur d'eau–eau.

On discute les implications pour le refroidissement des coeurs surchauffés de réacteurs nucléaires.

GEGENSTROM VON LUFT/WASSER UND DAMPF/WASSER DURCH EINE HORIZONTALE PERFORIERTE PLATTE

Zusammenfassung—Der Beginn des Eindringens von über einer perforierten Platte siedendem Wasser nach unten wurde sowohl mit aufwärtsgerichteten Luft- als auch Dampfströmungen untersucht. Empirisch wurde eine Bezugslänge für die Interpolation ermittelt, die-eingeführt in die Wallis-Gegenstrom-Gleichung-die Luft-Wasser-Messungen für eine Vielzahl von perforierten Plattengeometrien gut widergibt und auch für Messungen an einem Rohrbündel über die ganze Länge mit gesättigtem Wasser und Dampf anwendbar ist. Dieselbe Gleichunge paßt auch für die Dampf-Wasser-Messungen wenn sie entsprechend der Dampfkondensation in der unmittelbaren Umgebung der Platte korrigiert wird. Es werden Anwendungen für die Kühlung von überhitzten Atomreaktorkernen diskutiert.

ВСТРЕЧНОЕ ТЕЧЕНИЕ ВОЗДУХА-ВОДЫ И ПАРА-ВОДЫ ЧЕРЕЗ ГОРИЗОНТАЛЬНУЮ ПЕРФОРИРОВАННУЮ ПЛАСТИНУ

Аннотация — Исследовалось возникновение направленного вниз перемещения насыщенного пузырьками объема воды над перфорированной пластиной при восходящем течении воздуха и пара. Эмпирическим путем найдена интерполяционная длина масштабирования, введение которой в уравнение Уоллиса для противоточного движения позволяет хорошо описать данные, полученные для воздуха и воды при различных геометриях перфорированной пластины, также как и данные для пучка труб, заполненных насыщенной водой и паром. При соответствующем учете конденсации пара в непосредственной близости от пластины это уравнение также описывает данные, полученные для пара и воды. Рассмотрена возможность применения результатов исследования для охлаждения перегретых сердечников ядерного реактора.